Bioresources and Bioprocessing

RESEARCH

Open Access

Preparation of injectable hydrogel with near-infrared light response and photo-controlled drug release

Jianbo Zhao[1,2], Xingxing Liang[1], Hui Cao[1*] and Tianwei Tan[1]

Abstract

Photo-controlled release hydrogel provides a new strategy for treating tumours. Under the stimulation of external light sources, the ability to release the entrapped drug on time and space on demand has outstanding advantages in improving drug utilisation, optimising treatment, and reducing toxicity and side effects. In this study, a photo-controlled drug delivery system for disulphide cross-linked polyaspartic acid (PASP-SS) hydrogels encapsulating proteinase K (ProK) adsorbed with platinum nanoparticles (PtNPs) was designed. The injectable cysteamine-modified polyaspartic acid (PASP-SH) sol and PtNPs adsorbed by ProK (ProK-PtNPs) as regulatory factors were prepared. Then, ProK-PtNPs and lentinan were dissolved in the sol, and the oxidant was added to the matrix to form the gel in situ quickly after injection. Finally, the degradation of PASP-SS hydrogel by ProK and the controllability of drug release under near-infrared (NIR) light irradiation were elucidated. In vitro degradation of hydrogels and drug release experiments showed that the degradation rate of PASP-SS hydrogel significantly increased and the drug release rate increased significantly under near-infrared radiation. The results of cytotoxicity test showed that PASP-SS, ProK-PtNPs, and lentinan all had more than 90% cell survival rate on NIH3T3, and the lentinan released from the carrier obviously inhibited the proliferation of MCF7. PASP hydrogel has the potential to respond to on-demand light control.

Keywords: Polyaspartic acid hydrogel, Near-infrared light, On-demand degradation, Drug delivery, Photo-controlled release

Introduction

Injectable hydrogels have been developed over the past decades. Their high water content, biocompatibility, biodegradability, and in situ gel-sol conversion capabilities make them attractive in a variety of biomedical applications (Li et al. 2012, 2014; Huynh and Wylie 2019; Yang et al. 2019). Due to the injectable hydrogel delivery system, the drug and sol can be fixed at the target point by injection (Yesilyurt et al. 2016; Liu et al. 2017). After the gel is formed in situ, small molecules or macromolecular drugs are released through diffusion of the gel network, which can maintain local high concentrations of drugs for a long time to reduce the risk of side effects and patient discomfort (Singh and Lee 2014; Dong et al. 2016; Xing et al. 2016). Therefore, a great deal of research focuses on its potential application in targeted drug delivery; however, drug diffusion is generally passive or reliant on the natural degradation of hydrogels to release drugs: such drug release is not controllable and on-demand release is thus impossible. Currently, a common strategy is to give the drug delivery system the ability to receive signals spontaneously and rationally release the drug in response to environmental changes.

Stimuli-responsive hydrogels, also known as smart hydrogels, undergo significant changes in their swelling behaviour, network structure, permeability, or mechanical strength under external stimulation (Aimetti et al. 2009; Hu et al. 2011; Qiu et al. 2014), such as temperature

*Correspondence: caohui@mail.buct.edu.cn
[1] Beijing Key Laboratory of Biochemical Engineering, Beijing University of Chemical Technology, No. 15 Beisanhuan East Road, Chaoyang District, Beijing 100029, People's Republic of China
Full list of author information is available at the end of the article

(Tuncaboylu et al. 2011; Zheng et al. 2016), pH (Gharaie et al. 2018; Qu et al. 2018), light (Hu et al. 2017a, b; Liu and Liu 2019; Zhang et al. 2019), and electromagnetic fields (Shi et al. 2014). Therefore, when stimuli-responsive hydrogels are applied to a drug delivery system, the embedded drug can be released in a controlled manner. Light-responsive hydrogels are a type of stimuli-responsive hydrogel that is currently of widespread interest, with limited side effects because illumination is noninvasive and allows remote manipulation without additional reagents (Hu et al. 2017a, b; Lei et al. 2017). By adjusting the irradiation parameters, such as the illumination power density and the illumination time, the irradiation dose can be accurately controlled, so that the light reaction can be precisely controlled. Near-infrared (NIR) light has good tissue penetration and no phototoxicity to cells (Hu et al. 2017a, b; Raia et al. 2017). Therefore, NIR-responsive hydrogels are important in biomedical applications. For instance, the method of adjusting enzyme activity by NIR illumination is facile and feasible. It has been reported that platinum nanoparticles (PtNPs) within an enzyme allow local heating through the photothermal effect of the PtNPs upon NIR irradiation and consequently tailoring the enzyme activity (Wang et al. 2017).

Polyaspartic acid (PASP) hydrogel has excellent water absorption and water retention, biocompatibility and biodegradability, and can be applied in biosensors, drug delivery systems, and tissue engineering scaffolds (Zhao et al. 2005; Fujita et al. 2009; Liu et al. 2012; Quan et al. 2019). Thiol-modified PASP can achieve sol–gel reversible phase transitions as reported in the literature, with potential as a carrier for injectable hydrogel drug delivery systems (Zrinyi et al. 2013; Gyarmati et al. 2013, 2014). Moreover, the PASP backbone is destroyed by protease cleavage of the amide bond (Wang et al. 2016a, b; Han et al. 2018), causing the gel network to collapse and release the drug. Nevertheless, the uncontrollability of drug release limits the application of PASP hydrogel in injectable hydrogel delivery systems. As a consequence, cysteamine-modified polyaspartic acid (PASP-SH) sol and PtNPs could be prepared, and then, PtNPs were adsorbed and immobilised on the surface of proteinase K (ProK) to form regulatory elements. Then, the regulatory elements and drugs were encapsulated in the sol, and the injectable properties of the sol were used to gel in situ around the tumour under non-surgical conditions. Finally, the enzyme activity was tailored by local warming under NIR radiation to control the degradation of PASP hydrogel, so as to achieve the goal of controlling drug release.

Materials and methods

Materials

Polysuccinimide (PSI) was prepared by the Luoyang Cairun Environmental Protection Materials Co., Ltd (China): its purity was greater than 99%. Phosphate buffer solution (PBS), dimethylformamide (DMF) (A.R.), sodium borohydride (A.R.), and cysteamine hydrochloride (A.R.) were obtained from Beijing Chemical Industry Group (China). Imidazole (A.R.) and polyvinylpyrrolidone (PVP) (A.R.) from J & K Scientific (China) were used. Dibutylamine (DBA) (TCI, A.R.) and DL-dithiothreitol (DTT) (Fluka, purum) were bought from Aladdin. Chloroplatinic acid (A.R.) and proteinase K (ProK) (A.R., average diameter 12.7 nm) were purchased from Sigma-Aldrich (USA). All reagents and solvents were used without further purification.

Synthesis of disulphide cross-linked PASP (PASP-SS) gel and cysteamine-modified PASP (PASP-SH) sol

PASP-SS gel and PASP-SH sol were synthesised according to a previously reported procedure (Scheme 1) (Gyarmati et al. 2013). In a typical synthesis, 0.97 g PSI

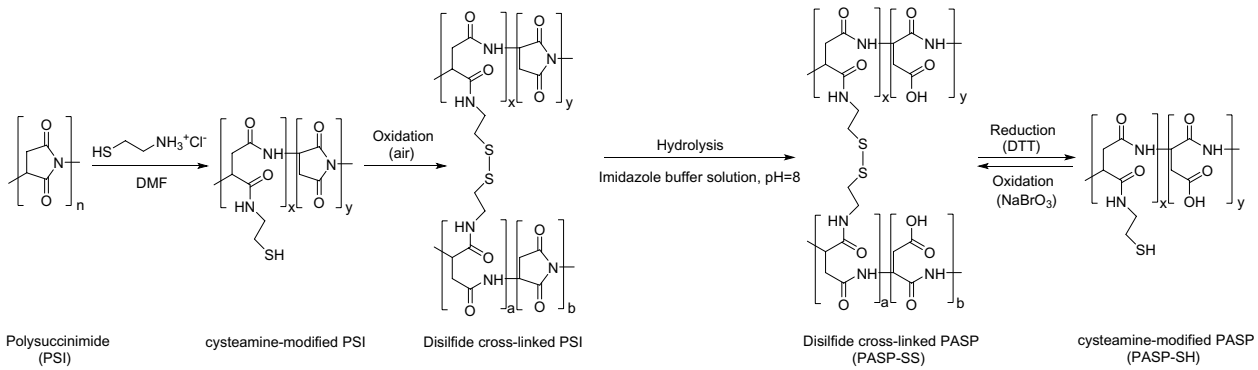

Scheme 1 Schematic illustration of the synthetic route to PASP-SS gel and PASP-SH sol preparation

(containing 10 mmol of succinimide repeating units) and 0.228 g (2 mmol) cysteamine hydrochloride were dissolved in DMF under a nitrogen atmosphere. 340 µL deprotonating agent DBA was added dropwise. After 3 h of reaction, the solution was transferred to a watch glass and the thiol side chain of the cysteamine-modified PSI was oxidised in air for 2 days to form disulphide bonds. The disulphide cross-linked PSI specimens were then subjected to ring-opening hydrolysis in imidazole buffer solution (at pH = 8) for 3 days to obtain PASP-SS gels. Finally, PASP-SS gels were dissolved in PBS solution with 10 mM DTT. After 15 min, it was completely dissolved and converted into PASP-SH sols. After purification by ultrafiltration, solid PASP-SH was obtained by lyophilisation, and the polymers were stored at 8 °C for analysis and later use.

The chemical structure of PASP-SH was confirmed by ^{1}H-NMR spectroscopy (AV-400 MHz, Bruker, USA). Twenty milligrams PASP-SH was dissolved in D_2O to a concentration of less than 5 mg/mL, and all spectra were recorded at 300 MHz using 128 scans. The spectroscopy signals were as follows: 4.88 (s, CH in succinimide rings); 4.60 (s, CH in aspartic acid and cysteamine-modified succinimide rings); 3.58 and 3.31 (m, m, CH_2 in cysteamine side chains); 2.94 and 2.70 (s, s, CH_2 in repeating units).

Preparation of PtNPs-ProK

PtNPs-ProK was prepared by the following two steps (Wang et al. 2016a, b): a mix of 2 mM chloroplatinic acid and 1.6 mM PVP in 10 mL aqueous solution was magnetically stirred at room temperature for 1 h. After that, excess sodium borohydride solution was slowly added dropwise and stirred while the specimen was stood in an ice water bath for 2 h. After multiple dialysis steps with deionised water, PtNPs stock solutions can be obtained. Then, we weighed 100 mg ProK, added a certain amount of 0.02 M PBS solution to prepare ProK solution, and then, we took 300 µL protease solution and 120 µL PtNPs stock solution and mixed them to obtain ProK embedded with PtNPs (PtNPs-ProK) for cryopreservation at 4 °C.

PASP-SS gel and PASP-SH sol physicochemical characteristics

Raman spectroscopy (VERTEX 70v, Bruker, Germany) was used to verify the thiol groups of PASP-SH and the disulphide bonds of PASP-SS. A small amount of lyophilised samples were plated on the slide and flattened using another clean slide. The spectrum ranged from 400 to 3500 cm^{-1}. The redox process of PASP-SS gel and PASP-SH sol was characterised by rheology. The 3 mL 10 wt% PASP-SH PBS solution was mixed with 0.22 M oxidant ($NaBrO_3$) solution and transferred to the sample stage of the rotary rheometer (AR2000ex, TA instruments, USA) to monitor the gel storage modulus G' and loss modulus G'' during the redox process. After the PASP-SS gel was reduced by DTT, 1 M $NaBrO_3$ solution was added for oxidation to monitor the storage modulus G' and loss modulus G'' of the secondary redox process. A constant angular frequency ($\omega = 10\ s^{-1}$) and constant strain (1%) were used.

Microscopy

The TEM images were collected using a transmission electron microscope (JEM2010, JEOL, Japan) with an accelerating voltage of 200 kV. PtNPs and PtNPs-ProK aqueous solution (0.2 mL; 1 wt%) was dispersed uniformly by ultrasonication; the solution was then adsorbed on copper grids with ultra-thin carbon film for 30 s and transferred to 3% uranium acetate for negative staining.

The images of ProK loaded on PtNPs were observed using a confocal laser scanning microscope (CLSM) (TCS SP5, Leica, Germany). DMSO solution containing fluorescein isothiocyanate was dripped into phosphoric acid buffer (pH = 9) containing 20 mg ProK and stirred for 4 h at room temperature in the dark. The reaction was terminated with 50 mmol/L NH_4Cl, dialysed with a dialysis bag (3 kD) for 48 h, and then lyophilised. The aforementioned powder was weighed to 10 mg, and 10 mg/mL ProK solution was prepared with PBS buffer solution. PtNPs-ProK was prepared by the aforementioned method ("Preparation of PtNPs-ProK" section), and the samples were then observed on the sample table.

Photothermal effect of PtNPs-ProK

1.5 mL ProK solution (10 mg/mL) was mixed with 0.6 mL PtNPs (50 µg/mL, 150 µg/mL, 300 µg/mL) and stored at 4 °C overnight. One millilitre samples were taken into the cuvette and irradiated by NIR laser (808 nm, New Industries Corp., Changchun, China) for 10 min at 1 W/cm^2, 1.5 W/cm^2, and 2 W/cm^2, respectively, and simultaneously the thermographs and temperatures were recorded using an infrared camera (Magnity Electronics, China) to evaluate the photothermal effect of PtNPs-ProK.

Assays to determine enzymatic activity of ProK

The enzymatic activity of ProK is defined as the amount of casein consumed by 1 g ProK per hour (Bignasca et al. 2011). ProK and PtNPs-ProK enzyme activities were determined by Coomassie Brilliant Blue staining. 0.1 mL PtNPs-ProK containing ProK (0.01 mg/mL) and PtNPs (0, 50 µg/mL and 150 µg/mL) was dissolved in 0.25 mL deionised water in the presence of 1 mg/mL casein. The reaction was processed with or without pulse NIR irradiation (1.5 W/cm^2) for 5 min, and the bulk temperature in solution was maintained at 37 °C in a water bath. Further, the remaining casein was stained with 5 mL Coomassie

Brilliant Blue solution (1 mg/mL). The absorbance of the reaction solution at 595 nm was measured using a UV spectrophotometer (Lambda35, PE, USA), and the enzyme activity was calculated by standard curve ($Y = 0.294X - 0.0025$; $R^2 = 0.9991$).

Formation and in vitro degradation of H-PtNPs-ProK

PtNPs-ProK (0.01 mg/mL ProK, 150 μg/mL PtNPs) was dissolved in an aqueous solution of PASP-SH at a concentration of 10 wt%. After incorporation into aqueous solution of oxidising agent (1 M $NaBrO_3$ in PBS), hydrogel loaded with PtNPs-ProK (H-PtNPs-ProK) was formed in situ in 2 to 4 min.

H-PtNPs-ProK gelatinised on a glass-surface vessel was placed in incubator at 37 °C. Irradiation with an NIR laser at 808 nm was conducted at a density of 1.5 W/cm^2, and photographs were taken at intervals of 30 min. Meanwhile, the storage G' and loss G'' moduli of irradiated and non-irradiated portions were measured by a rotational rheometer.

Drug release behaviour test

As a drug model, 1 mg/mL lentinan and PtNPs-ProK were dissolved in PASP-SH in PBS solution and then oxidised into gel. Since the drug was embedded in the gel by oxidation of the aqueous polymer solution, the disadvantage of low encapsulation efficiency of the conventional drug adsorption method was avoided (Van et al. 2016).

The effect of NIR light on drug release was investigated: 0.1 g H-PtNPs-ProK-loaded lentinan was placed in the standard PBS solution. The absorbance of PBS solution was measured by UV spectrometer at 490 nm over 21 h. Thereafter, NIR light (1.5 W/cm^2, blocked by chicken flesh with a thickness of 30 mm) was used to irradiate the PBS solution for 2 h, and the PBS solution was taken out at intervals to measure absorbance at 490 nm. Meanwhile, the effect of first NIR illumination on drug release in vitro was also analysed in the same way. 0.1 g H-PtNPs-ProK was placed in PBS standard solution and irradiated with NIR light for 2 h (1.5 W/cm^2, blocked by chicken flesh with thickness of 30 mm). The PBS solution was taken and measured by a UV spectrometer at 490 nm at regular intervals. After NIR light was removed, the absorbance of the PBS solution was recorded over 23 h. In addition, the effect of intermittent NIR irradiation on drug release in vitro was also investigated. The drug release rate was calculated by standard curve ($Y = 0.0033X + 0.079$; $R^2 = 0.996$).

To evaluate the activity of the released lentinan, PBS solution soaked with H-PtNPs-ProK after NIR (1.5 W/cm^2, blocked by chicken flesh with a thickness of 30 mm) irradiation for different times (0.5, 1, 1.5, 2, and 2.5 h) was transferred to a 96-well plate inoculated with MCF7 cells at 37 °C. After 48 h of culture, cell viability was determined by a standard cholecystokinin octapeptide (CCK-8) assay, and each assay was repeated six times.

In vitro cytoactive assays

NIH3T3 (a mouse embryonic fibroblast cell line) and MCF7 (a human breast cancer cell line) cells were regularly cultured in DMEM supplemented with 10% foetal bovine serum (GIBCO Inc.), 100 units/mL penicillin, and 100 mg/mL streptomycin at 37 °C with 5% CO_2 in a humidified incubator.

The cytotoxicity of carrier materials (PASP-SH sol, sodium bromate), Prok-PtNPs, and lentinan on NIH3T3 cells was analysed. The cells were seeded in 96-well plate at a density of 1×10^5 cells per well and incubated in an incubator at 37 °C for 24 h. PASP-SH sol, Prok-PtNPs, sodium bromate, and lentinan at different concentrations (0, 1, 10, 50, and 100 μg/mL) were added to the wells and cultured for 24 h, respectively. After that, the cell viability was determined by cholecystokinin octapeptide (CCK-8) assay (six replicates in each group).

Results and discussion

Sol-to-gel transition

Raman spectroscopy was used to monitor the dissolution of PASP-SS gel induced and the re-gelation of PASP-SH sol by redox (Gyarmati et al. 2014). As can be seen from Fig. 1a, the disulphide peak of oxidised PASP-SS appears at 510 cm^{-1}, and its strength decreases in the reduced PASP-SH, while the mercaptan peak at 2571 cm^{-1} only appears in the reduced state. We enlarged Fig. 1a from 400 to 800 cm^{-1} to get Fig. 1b: another characteristic mercaptan peak at 661 cm^{-1} can also distinguish the redox state, but partly overlaps with the characteristic peak of PASP at 640 cm^{-1}, which is not obvious. Thus, we conclude that the sol–gel transition of PASP-SS/PASP-SH network is caused by a redox reaction.

Since rheological properties are particularly sensitive to molecular weight, rotation rheometers are often used to observe the cross-linking process in polymers. With the increase in degree of cross-linking, the molecular weight of the polymer increased, and the macroscopic behaviour was such that the fluidity of the polymer was decreased, gelation occurred, and the storage modulus G' also increased (Treece et al. 2007). The gelation time is estimated from the change of storage modulus with time and is defined as the inflection point-reaction time function of the storage modulus (Fig. 1c). The oxidant $NaBrO_3$ was added to PASP-SH polymer aqueous solution, and the gelation time was 250 ± 5 s. The hydrogel PASP-SS was dissolved by the reducing agent DTT and then dosed with an excess of oxidant $NaBrO_3$ to cross-link the polymer again. The gelation time was 260 ± 7 s.

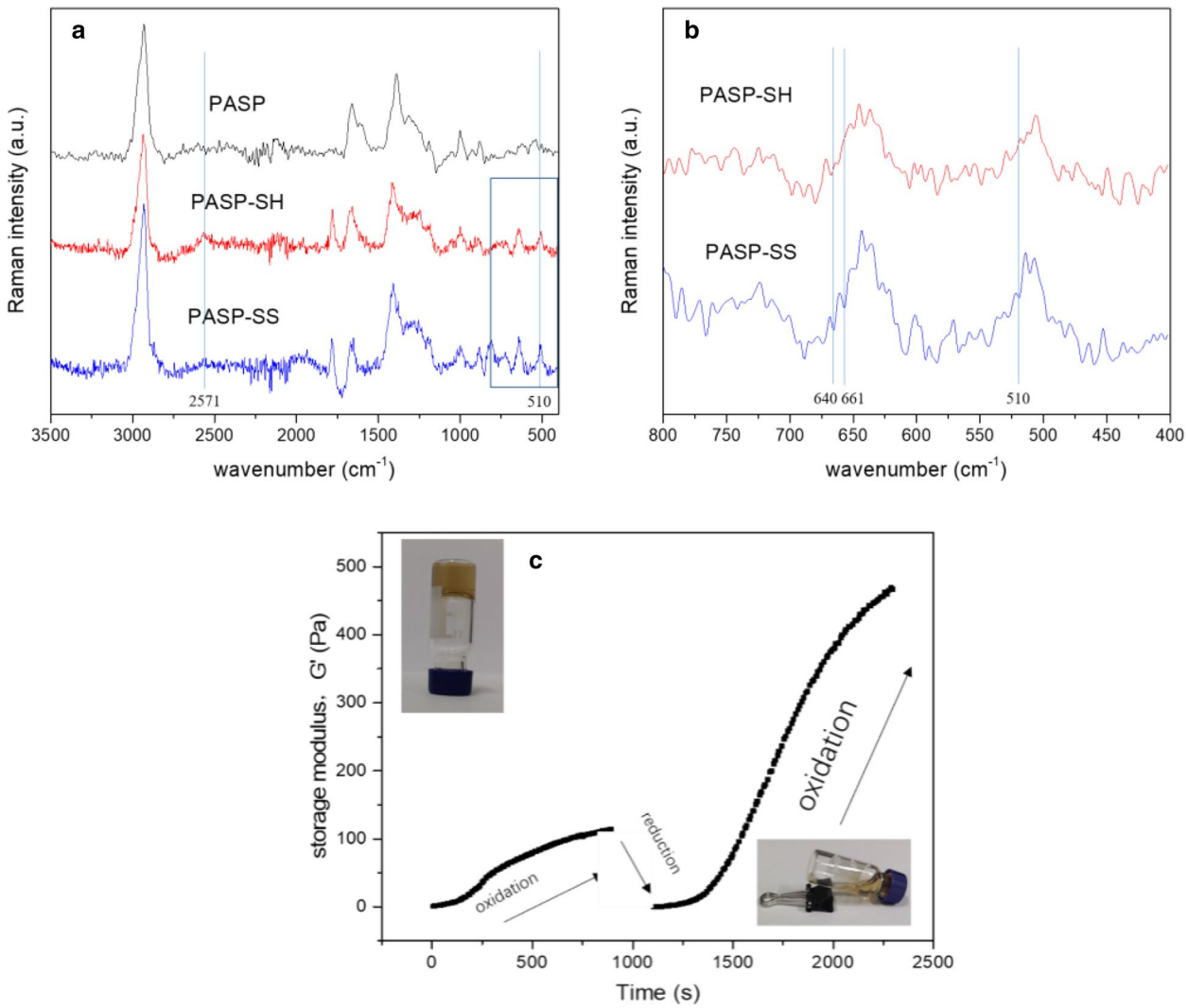

Fig. 1 Raman spectra and sol–gel transition of PASP-SH and PASP-SS. **a** Raman spectra of PASP, reduced state PASP-SH and oxidised state PASP-SS; **b** detailed spectra of PASP-SH and PASP-SS in the range of 400–800 cm^{-1}; **c** rotating rheology measurement of reversible redox-induced sol–gel transition of PASP-SH; the upper left illustration shows oxidised PASP-SS gel, and the lower right illustration shows reduced PASP-SH sol

During the second oxidation process, the storage modulus *G′*, which is much greater than that after the first oxidation reaction, was due to the greater cross-linking of disulphide bonds formed by excessive oxidants during the second oxidation process. The results of Raman spectroscopy and rheological characterisation together confirmed the reversible redox reaction of PASP-SH in aqueous medium.

Characterisation of PtNPs-ProK

The morphologies of PtNPs and PtNPs-ProK were observed by TEM (Fig. 2). The hydrophilic groups on PVP can promote the dispersion of PtNPs and avoid the risk of continuous growth and agglomeration of PtNPs (Amyab et al. 2016). It can be seen that PtNPs are about 3–5 nm in size, spherical in shape, uniform in structure, and well dispersed (Fig. 2a). Figure 2b, c shows SEMs of PtNPs-ProK at different scales. Uranium peroxide negatively stained ProK showed poorer contrast, and the PtNPs were seen as black particles adsorbed on the irregular ProK. The particle size of ProK was about 10–20 nm. There were several PtNPs adsorbed on the same ProK, which might adversely affect subsequent photothermal conversion. The part marked within the red circle is ProK without a lattice, while PtNPs with a thin lattice appear around it (Fig. 2c).

In addition, the loading of PtNPs on ProK was also observed using CLSM (Fig. 3). PtNPs show blue light at

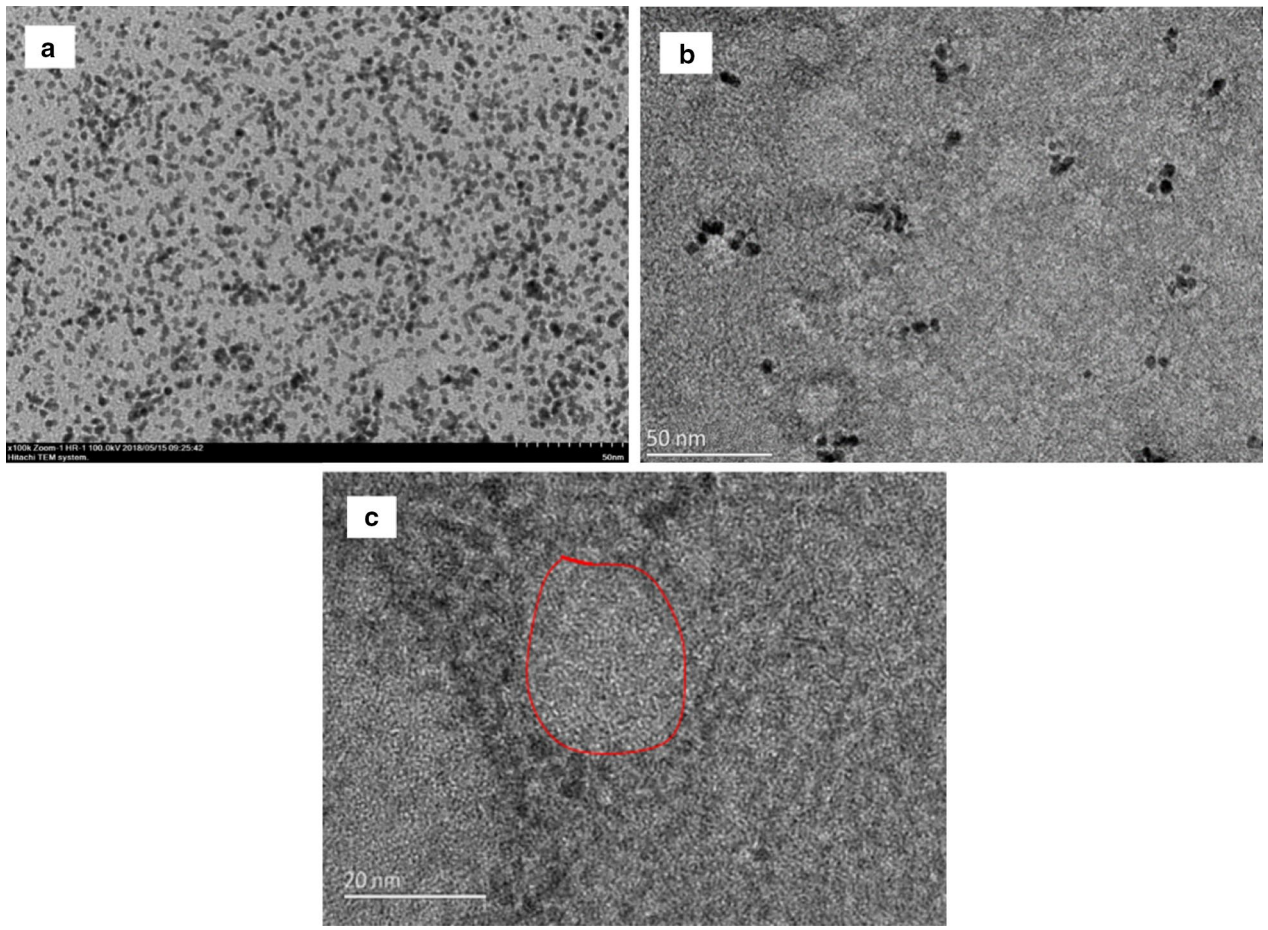

Fig. 2 TEM images of PtNPs **a** and PtNPs-ProK **b**, **c** at different scales, where **b**, **c** sample was negatively dyed, **c** the shape inside the red line is ProK

405 nm excitation (Fig. 3a), while FITC-labelled ProK shows green light when excited at 488 nm (Fig. 3b). It can be seen that blue light and green light appeared at similar positions, and from the superposition of Fig. 3a–b, Fig. 3b shows that blue light surrounds the green light, evincing the adsorption of PtNPs around Prok. Due to the brightness, some ProK is covered by brighter blue light, and PtNPs-ProK agglomerated on the glass slide because of water evaporation, but it still showed that Prok adsorbed most of the PtNPs.

NIR-triggered photothermal conversion and enzyme release of PtNPs-ProK

To monitor the temperature variation of PtNPs-ProK under NIR irradiation, we took photographs at different times using an infrared camera to explore the effects of different PtNPs concentrations and infrared power densities on PtNPs-ProK temperature. The temperature change in PtNPs-ProK was mainly affected by PtNPs concentration, infrared power density, and irradiation time (Fig. 4a). When the concentration of PtNPs is constant, the temperature rise in PtNPs-ProK increases with increasing infrared power density and prolonged irradiation time (Fig. 4b); when the concentration of PtNPs increases, the temperature rise also increased (Fig. 4c, d). It is noteworthy that when the infrared radiation exposure exceeded 5 min, the temperature did not change significantly. Considering that the human body temperature is 37 °C and the optimum temperature of ProK is 57 °C (Miyazaki et al. 2000), the optimum concentration of PtNPs, infrared power density, and irradiation time should be chosen when the temperature range is about 20 °C, that is, the concentration of PtNPs is 150 ug/mL, the power density is 1.5 W/cm^2 and the irradiation time is 5 min.

ProK and PtNPs-ProK activities were determined by Coomassie Brilliant Blue staining. ProK (0.01 mg/mL, 0.03 mg/mL, and 0.05 mg/mL) activity was determined at 37 °C and 57 °C, respectively. As can be seen

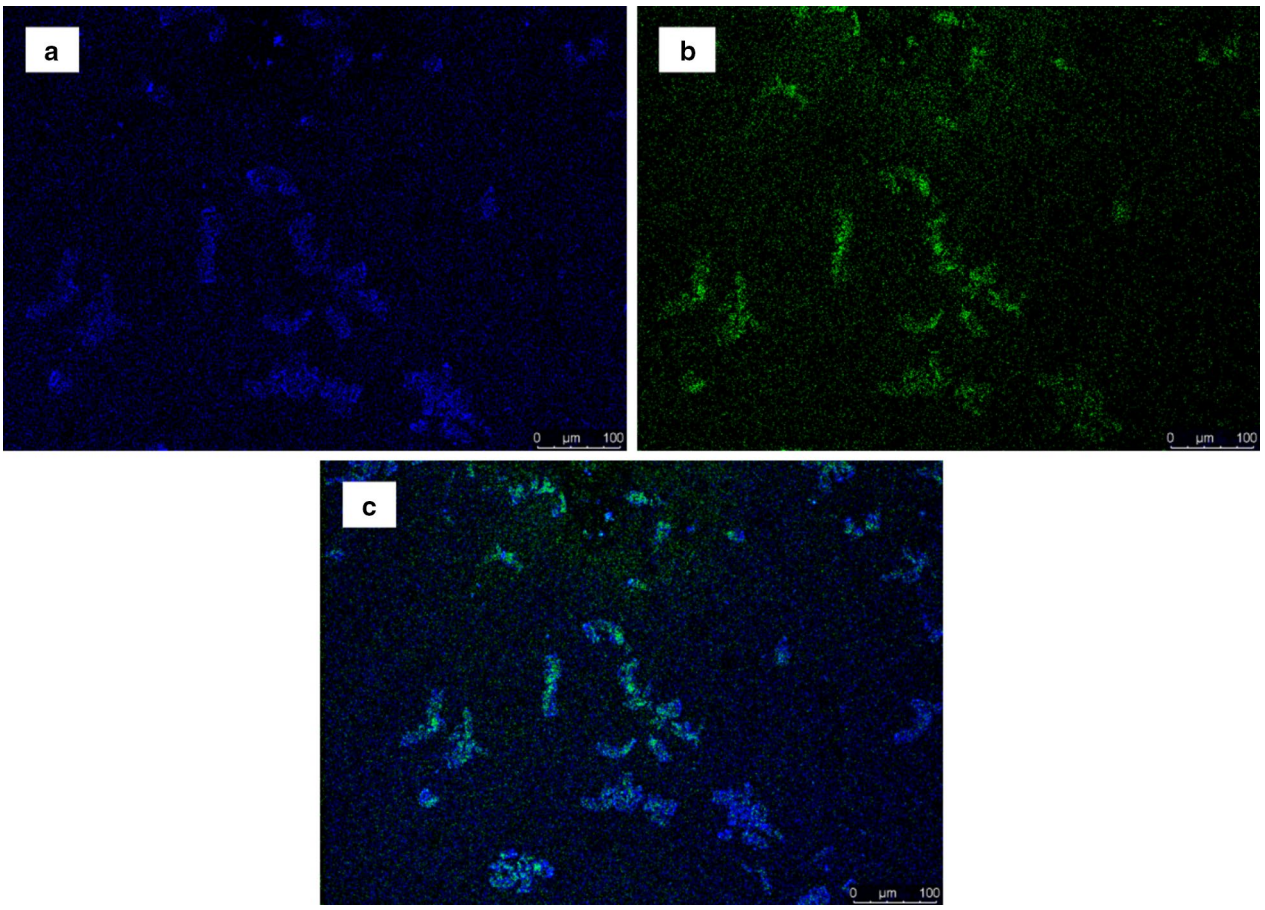

Fig. 3 Laser scanning confocal microscopy photographs of PtNPs-ProK at 405 nm (**a**), 488 nm (**b**), and (**c**) overlaying (**a**) and (**b**)

from Fig. 5a, the difference in the activity of 0.01 mg/mL ProK is more than 2.5 times greater, while that of 0.05 mg/mL is less than 1.2 times greater. This is due to the fact that the 0.05 mg/mL ProK is too similar to the substrate. The rate of later reaction declined, even if enzymatic activity increased, it was still affected by an insufficiency of substrates, while enzymes at 0.01 mg/mL were always under conditions with sufficient substrate. Therefore, 0.01 mg/mL ProK was selected for further determination of the effect of NIR on enzyme activity. Figure 5b shows changes in enzyme activity of PtNPs-ProK containing different concentrations of PtNPs with and without NIR irradiation (1.5 W/cm^2, 5 min) at 37 °C. It can be seen that the activity of ProK without PtNPs changed little before and after infrared irradiation, but the activity of PtNPs-ProK with 150 ug/mL PtNPs increased more than threefold under non-infrared irradiation and infrared irradiation. NIR irradiation can significantly improve enzyme activity in PtNPs-ProK.

NIR-triggered H-PtNPs-ProK degradation in vitro

To verify the regulatory role of PtNPs-ProK in the gel network, the H-PtNPs-ProK was immersed in a water bath maintained at 37 °C and irradiated by infrared laser. The hydrogel was photographed at intervals of 30 min, and storage modulus G' and loss modulus G'' were measured on irradiated and non-irradiated areas. Degradation of H-PtNPs-ProK in vitro was characterised by the rheological properties. From Fig. 6, it can be seen that the non-irradiated part of H-PtNPs-ProK is always transparent and flat, and the storage modulus G' and loss modulus G'' were unchanged; while there is a depression (marked by the red lines) in the NIR-irradiated area of H-PtNPs-ProK, the colour thereof is darker and the viscoelasticity decreases greatly in that region. This shows that NIR irradiation can significantly accelerate the cleavage of the amide bond on the main chain of PASP-SS by ProK, resulting in disintegration of the cross-linked network.

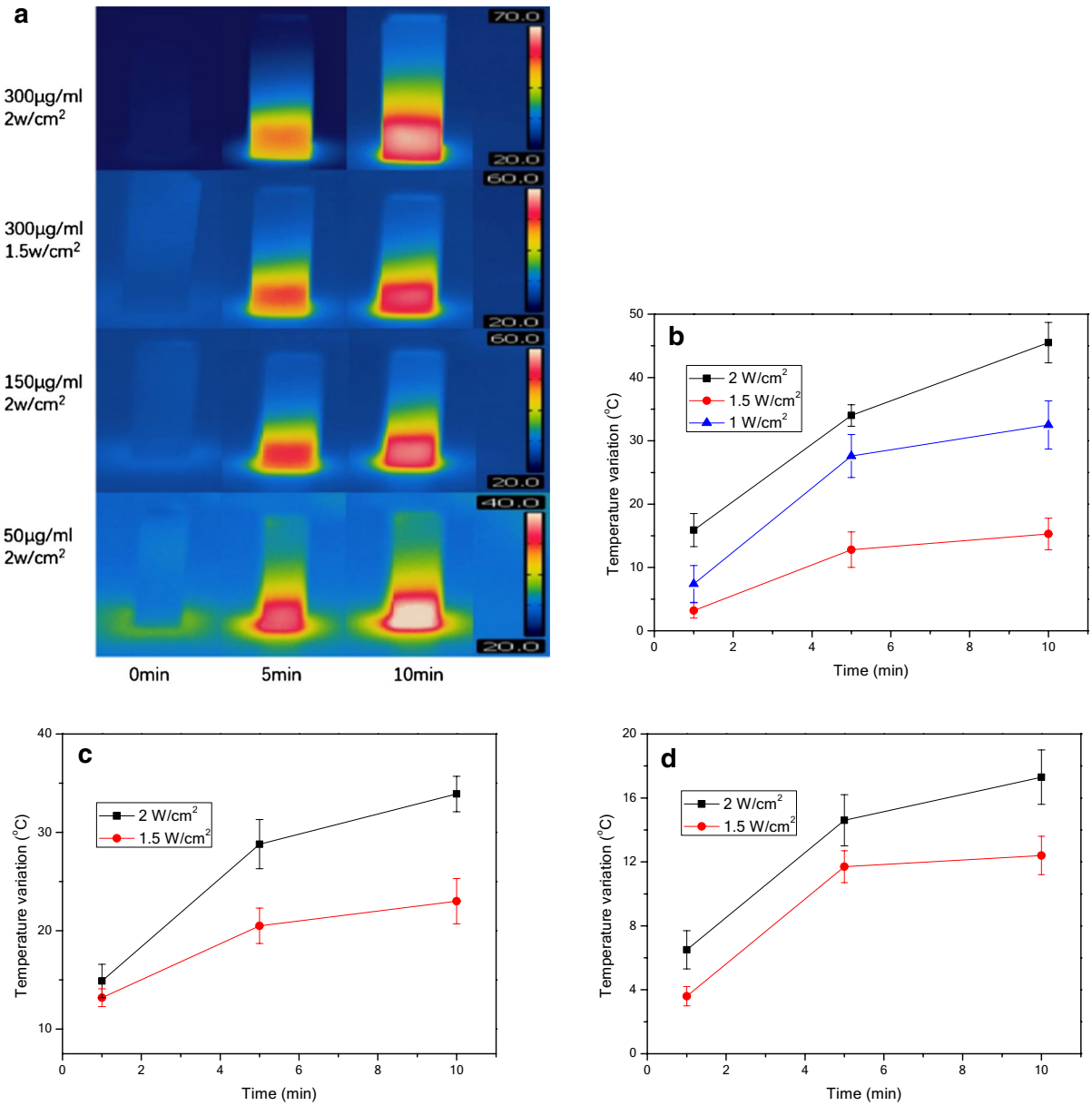

Fig. 4 NIR-triggered photothermal conversion and enzyme release of PtNPs-ProK. **a** Thermographs by infrared laser on PtNPs-ProK under different contents of PtNPs and different infrared power densities; effect of different infrared power densities on temperature changes of PtNPs-ProK solution at a concentration of 300 μg/mL PtNPs (**b**), 150 μg/mL PtNPs (**c**), and 50 μg/mL PtNPs (**d**)

NIR-triggered drug release

The effects of NIR irradiation on drug release were investigated by post-infrared irradiation, pre-infrared irradiation, and intermittent infrared irradiation, respectively. A chicken flesh specimen with a thickness of 30 mm was placed between the infrared laser and the hydrogel to simulate muscle blockade, and the drug-loaded H-PtNPs-ProK was irradiated by infrared radiation (power density 1.5 W/cm^2). The drug release rate changed with time as shown in Fig. 7. After the drug release reached equilibrium without infrared irradiation, the amount of drug released increased significantly under the infrared irradiation (Fig. 7a). This was mainly due to the enhanced activity of ProK under infrared irradiation, which accelerated gel degradation and re-released the drug. Drug release by pre-infrared irradiation can reach its peak rapidly. After stopping infrared irradiation, drug release does not increase with

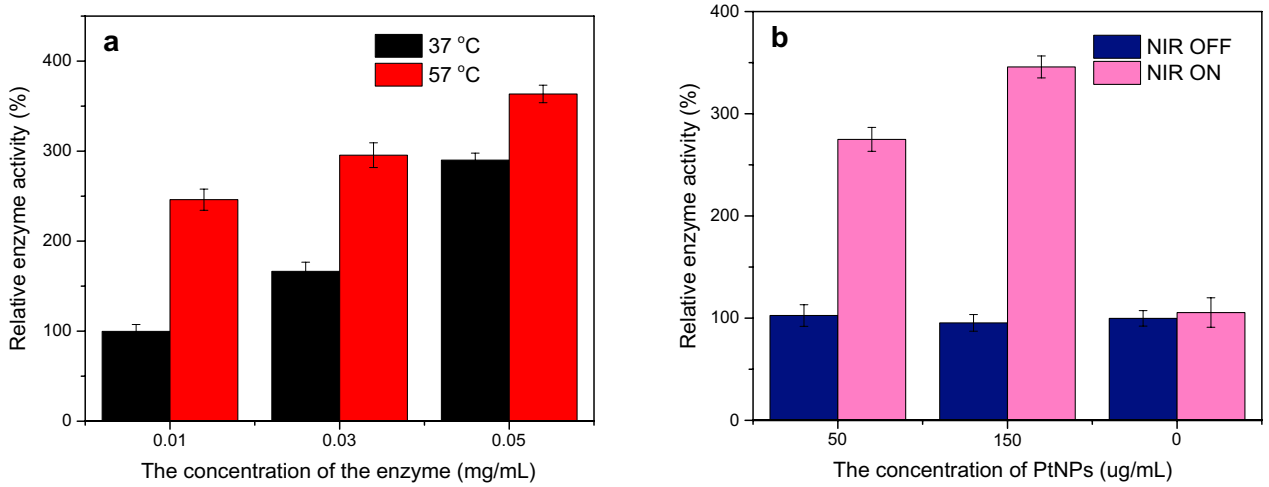

Fig. 5 **a** Activity of ProK with different concentrations at 37 and 57 °C, respectively; **b** the effect of PtNPs-ProK with different PtNPs concentration on enzyme activity under infrared irradiation or not

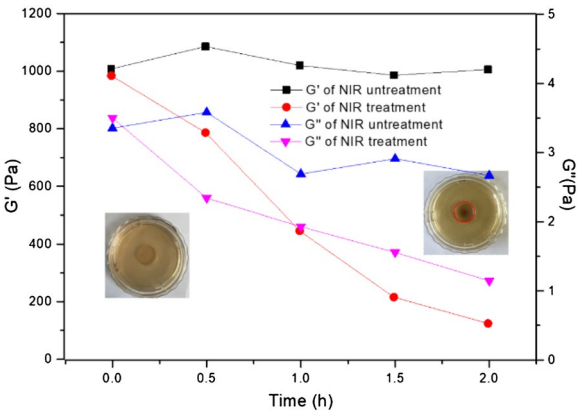

Fig. 6 Storage modulus *G´* and loss modulus *G´´* of H-PtNPs-ProK with time; the left-hand photograph shows H-PtNPs-ProK without irradiation: the right-hand photograph shows H-PtNPs-ProK after 2 h of NIR irradiation

time and even shows a slight downward trend (Fig. 7b). This may be related to dilution of drug concentration by buffer replaced during sampling. When the infrared light was intermittently applied, the release rate was significantly faster than that without irradiation. In time, the drug release slowed down. After 800 min, intermittent irradiation with infrared light resulted in the rapid release of the drug again (Fig. 7c). This was mainly due to the fact that ProK catalyses the gel network to become loose after a period of time, and the infrared irradiation increases enzyme activity (Han et al. 2018), so that the drug is rapidly released again; therefore, the amount of drug released by hydrogel under infrared radiation is much greater than that under non-infrared radiation in the same time and exhibited a faster release rate. NIR radiation can thus tailor drug release.

In vitro cell studies of H-PtNPs-ProK

The cytotoxicity of NIH3T3 and MCF7 was evaluated by CCK-8 method. Since H-PtNPs-ProK has no fluidity, it is difficult to mix the medium uniformly, and the cells grow slowly and do not readily adhere to the wall. Therefore, PASP-SH, the precursor of H-PtNPs-ProK, and the oxidant sodium bromate were selected to evaluate the cytotoxicity of NIH3T3. The cytotoxicity of PASP-SH, oxidant sodium bromates, ProK-PtNPs, and lentinan against NIH3T3 is shown in Fig. 8. The cell survival rate exceeded 90% at all other concentrations, except for about 70% at a sodium bromate solution concentration of 200 μg/mL (Fig. 8a, b). This indicates that the raw materials of the gel carrier have no obvious killing effect on NIH3T3, which further indicates that H-Pt-ProK can be used as a carrier for drug loading. In addition, the cytotoxicity of ProK-PtNPs and lentinan was evaluated. Cell viability was found to be higher than 80% (Fig. 8c, d), indicating that the carrier and drug injected into the human body have no obvious killing effect on the cells, and can be used as a drug delivery system. The effect of PASP-SH on the morphology of NIH3T3 cells was observed by optical microscopy. NIH3T3 cells appeared strip-like or triangular when cultured in complete medium with a small amount of shrinkage and agglomeration thereof (Fig. 8e); most of the NIH3T3 cells were still strip-like or triangular when cultured in complete medium with PASP-SH (Fig. 8f). These results suggest that PASP-SH has little effect on the proliferation of NIH3T3 cells.

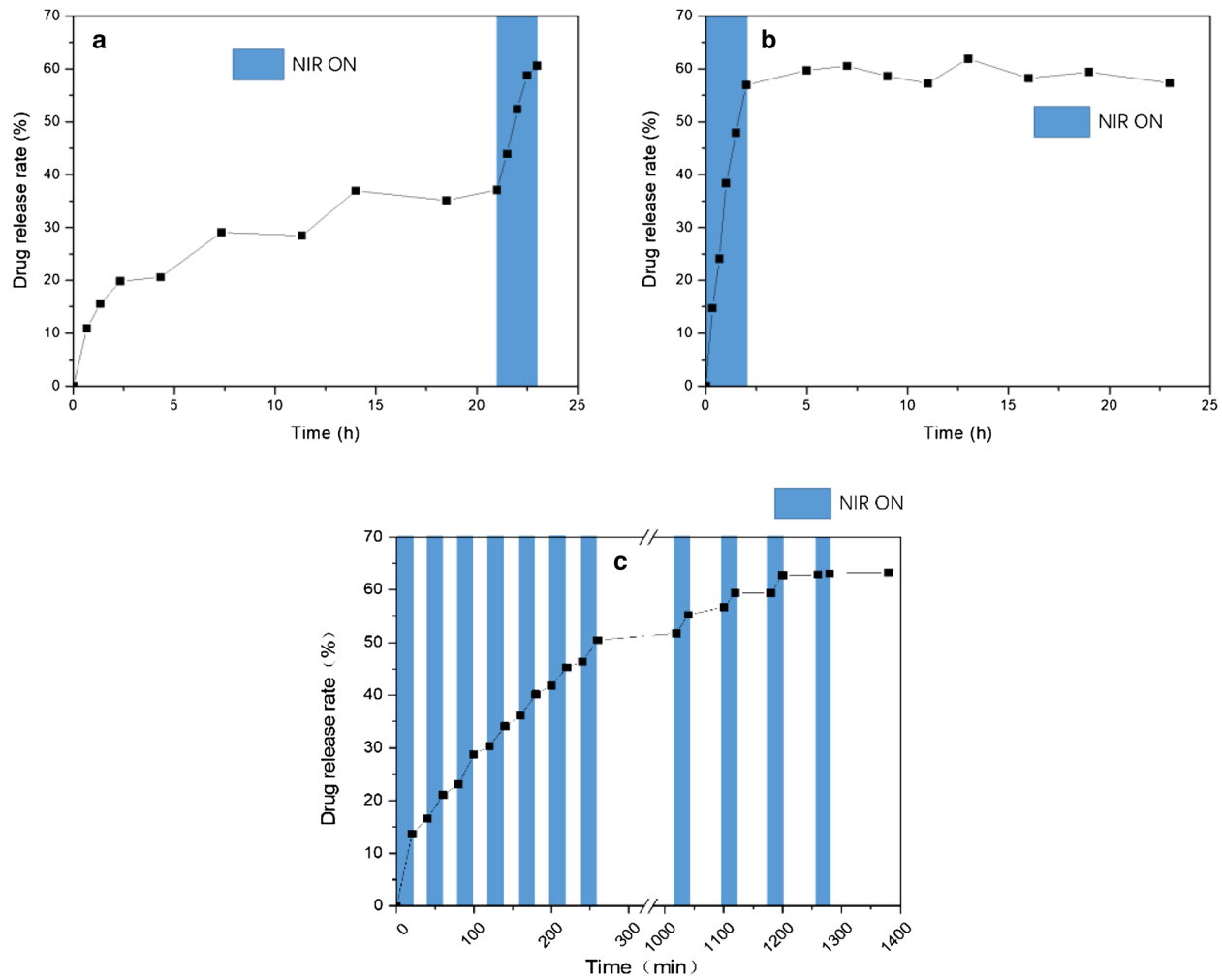

Fig. 7 In vitro release curve of lentinan under **a** post-infrared, **b** pre-infrared irradiation, and **c** intermittent infrared irradiation

Lentinan released from H-PtNPs-ProK irradiated by NIR light (power density 1.5 W/cm^2 over irradiation times of 10, 20, 30, 40, 50, and 60 min, respectively) was collected. The concentration was measured and formulated into a medium. MCF7 cells were cultured in the medium for 24 h to test the toxicity of lentinan to MCF7 cells (Fig. 9a). As the infrared irradiation time was increased, the concentration of lentinan in the medium increases, and the cell survival rate decreases significantly. It is foreseeable that the drug released by H-PtNPs-ProK after infrared irradiation could significantly inhibit the proliferation of MCF7. The morphology of MCF7 was observed by optical microscopy. The cells cultured in complete medium were spherical or elliptical (Fig. 9b where the orange line marks) on the wall of the culture flask, and a small number of apoptotic cells were irregularly elliptical or bubble (Fig. 9b where the red line marks) appeared inside the cells. When the drug released by H-PtNPs-ProK was added to the culture medium, most of the cells appeared elliptical (with eccentricity), and the number of apoptotic and ruptured cells was much greater than that before adding lentinan (Fig. 9c).

Conclusions

PASP-SS hydrogel and ProK-PtNPs were synthesised, and the injectability was achieved by the redox characteristics of hydrogel disulphide bonds and the rapid conversion of sol to gel. In addition, the photothermal effect of PtNPs was utilised to generate heat to enhance ProK activity through NIR irradiation, thereby accelerating the degradation of the hydrogel to control drug release. The CCK-8 method was used to demonstrate the cytotoxicity of the carrier materials and drugs on NIH3T3 and MCF7 cells. The results showed that the carrier materials and drugs were not toxic to NIH3T3, while the drug released from H-PtNPs-ProK inhibited the proliferation

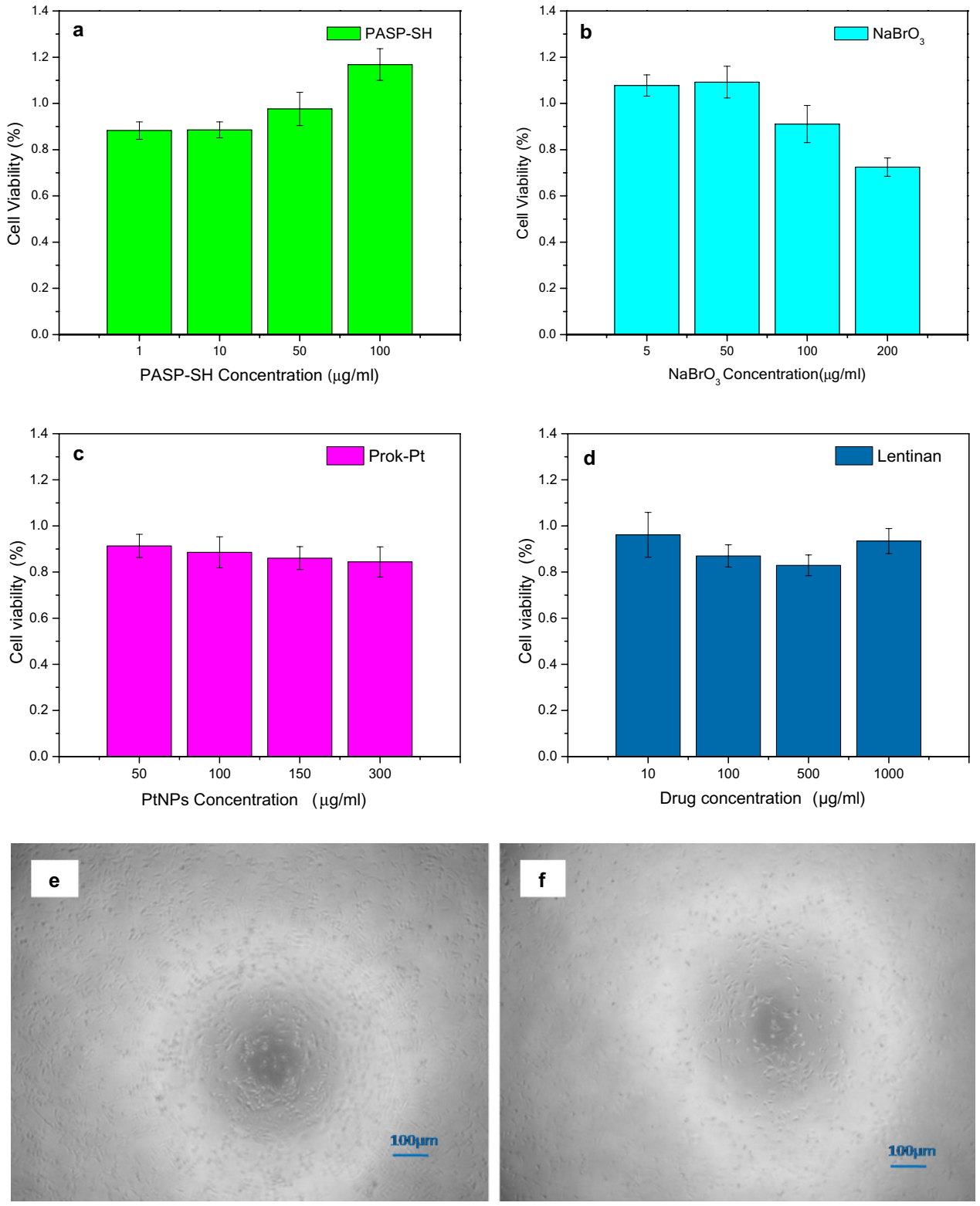

Fig. 8 The results of cytotoxicity test. Cytotoxicity of PASP-SH (**a**), sodium bromates (**b**), ProK-PtNPs (**c**), and lentinan (**d**) to NIH3T3, respectively; front (**e**) and back (**f**) morphology of PASP-SH-loaded NIH3T3

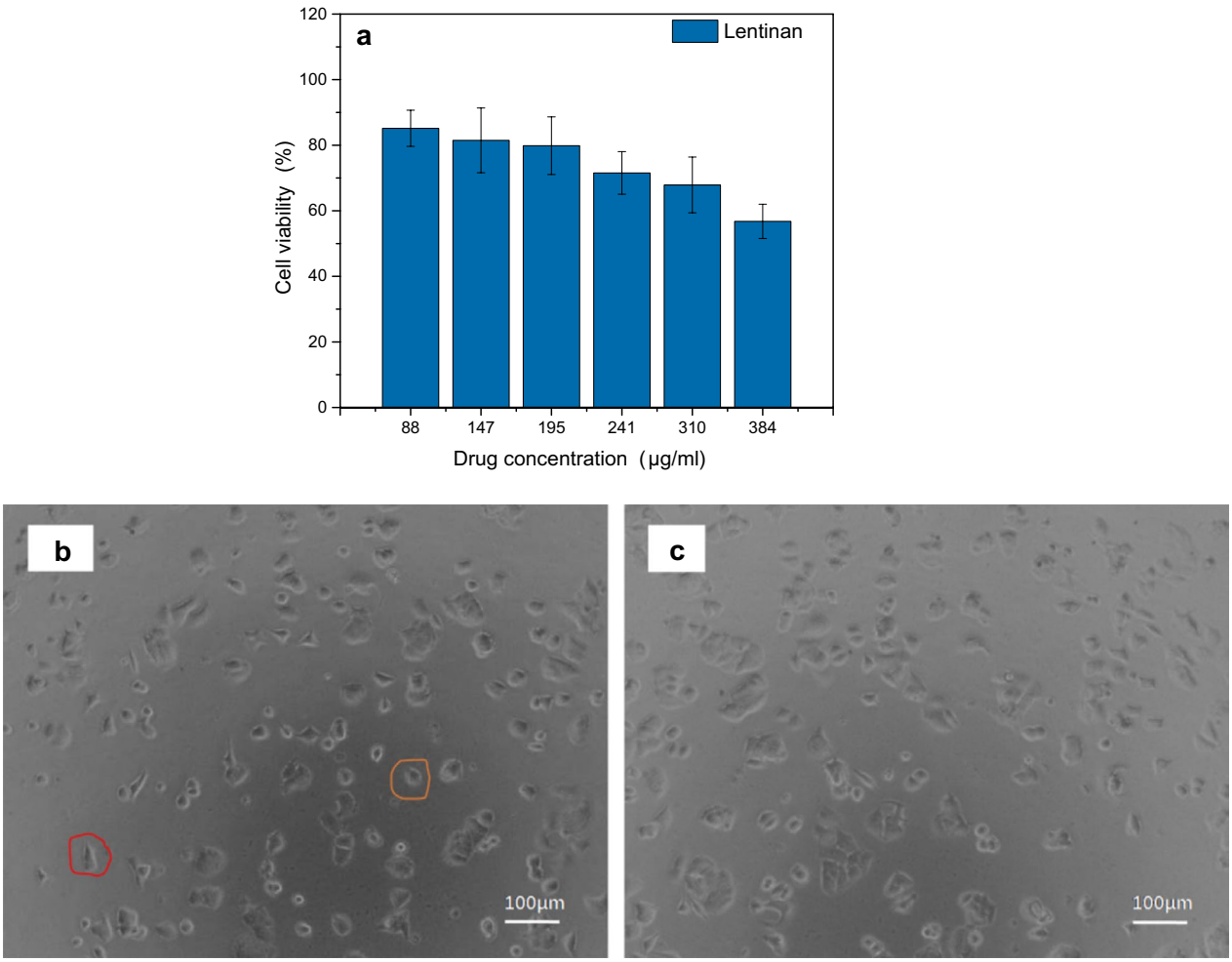

Fig. 9 The results of cytotoxicity test. **a** Cytotoxicity of lentinan to MCF7; front (**b**) and back (**c**) morphology of lentinan-loaded MCF7

of MCF7. Thus, we successfully constructed an injectable in situ gel-forming drug delivery system that can control the degradation of the gel by NIR irradiation to achieve on-demand release of the drug. This study will facilitate the design and development of novel controlled drug delivery systems.

Abbreviations

PASP: polyaspartic acid; PASP-SS: disulphide cross-linked polyaspartic acid; PASP-SH: cysteamine-modified polyaspartic acid; ProK: proteinase K; PtNPs: platinum nanoparticles; ProK-PtNPs: PtNPs adsorbed by ProK; NIR: near-infrared light; H-PtNPs-ProK: hydrogel loaded with PtNPs-ProK.

Acknowledgements

This article has received professional writing services from C. A. Fairfield.

Authors' contributions

ZJB contributed to the preparation of the manuscript. LXX contributed to the preparation and of injectable gels and platinum nanoparticles. CH contributed to the general advice and improving of the manuscript. All authors read and approved the final manuscript.

Funding

All sources of funding for this study are the National Natural Science Foundation of China (Grant No. 21865026), Xinjiang Production and Construction Corps Project (2018BC005), Hebei Key Research and Development Project (18273401D), and Hebei Province's Innovation Capacity Improvement Project (18952814D).

Availability of data and materials

Not applicable

Ethics approval and consent to participate

Not applicable.

Consent for publication

All authors agree to publish.

Competing interests

The authors declare that they have no competing interests.

Author details

[1] Beijing Key Laboratory of Biochemical Engineering, Beijing University of Chemical Technology, No. 15 Beisanhuan East Road, Chaoyang District, Beijing 100029, People's Republic of China. [2] Engineering Laboratory of Chemical Resources Utilization in South Xinjiang of Xinjiang Production

and Construction Corps, College of Life Sciences, Tarim University, Alar, Xinjiang 843300, People's Republic of China.

Received: 7 October 2019 Accepted: 20 December 2019
Published online: 03 January 2020

References

Aimetti AA, Machen AJ, Anseth KS (2009) Poly(ethylene glycol) hydrogels formed by thiol-ene photopolymerization for enzyme-responsive protein delivery. Biomaterials 30(30):6048–6054

Amyab SP, Saievar-Iranizad E, Bayat A (2016) Platinum nanoparticles with superacid-doped polyvinylpyrrolidone coated carbon nanotubes: electrocatalyst for oxygen reduction reaction in high-temperature proton exchange membrane fuel cell. RSC Adv 48(6):41937–41946

Bignasca A, Ianni C, Magi E, Rivaro P (2011) Using proteolytic enzymes to assess metal bioaccessibility in marine sediments. Talanta 86:305–315

Dong R, Zhao X, Guo B, Ma PX (2016) Self-healing conductive injectable hydrogels with antibacterial activity as cell delivery carrier for cardiac cell therapy. ACS Appl Mater Inter 8(27):17138–17150

Fujita Y, Mie M, Kobatake E (2009) Construction of nanoscale protein particle using temperature-sensitive elastin-like peptide and polyasparticacid chain. Biomaterials 30(20):3450–3457

Gharaie SS, Dabiri SMH, Akbari M (2018) Smart shear-thinning hydrogels as injectable drug delivery systems. Polymers. https://doi.org/10.3390/polym10121317

Gyarmati B, Vajna B, Némethy A, László K, Szilágyi A (2013) Redox- and pH-responsive cysteamine-modified poly(aspartic acid) showing a reversible sol-gel transition. Macromol Biosci 13(5):633–640

Gyarmati B, Krisch E, Szilágyi A (2014) In situ oxidation-induced gelation of poly(aspartic acid) thiomers. React Funct Polym 84:29–36

Han J, Zhao X, Xu W, Wang W, Han Y, Feng X (2018) Effect of hydrophobic polypeptide length on performances of hermo-sensitive hydrogels. Molecules. https://doi.org/10.3390/molecules23051017

Hu J, Hiwatashi K, Kurokawa T, Liang SM, Wu ZL, Gong JP (2011) Microgel-reinforced hydrogel films with high mechanical strength and their visible mesoscale fracture structure. Macromolecules 44(19):7775–7781

Hu J, Chen Y, Li Y, Zhou Z, Cheng Y (2017a) A thermo-degradable hydrogel with light-tunable degradation and drug release. Biomaterials 112:133–140

Hu J, Quan Y, Lai Y, Zheng Z, Hu Z, Wang X, Dai T, Zhang Q, Cheng Y (2017b) A smart aminoglycoside hydrogel with tunable gel degradation, on-demand drug release, and high antibacterial activity. J Control Release 247:145–152

Huynh V, Wylie RG (2019) Displacement affinity release of antibodies from injectable hydrogels. ACS Appl Mater Inter. https://doi.org/10.1021/acsami.9b12572

Lei K, Chen Y, Wang J, Peng X, Yue L, Ding J (2017) Non-invasive monitoring of in vivo degradation of a radiopaque thermoreversible hydrogel and its efficacy in preventing post-operative adhesions. Acta Biomater 55:396–409

Li Y, Rodrigues J, Tomas H (2012) Injectable and biodegradable hydrogels: gelation, biodegradation and biomedical applications. Chem Soc Rev 41(6):2193–2221

Li L, Wang N, Jin X, Deng R, Nie S, Sun L, Wu Q, Wei Y, Gong C (2014) Biodegradable and injectable in situ cross-linking chitosan-hyaluronic acid based hydrogels for postoperative adhesion prevention. Biomaterials 35(12):3903–3917

Liu Q, Liu L (2019) Novel light-responsive hydrogels with antimicrobial and antifouling capabilities. Langmuir 35(5):1450–1457

Liu M, Su H, Tan T (2012) Synthesis and properties of thermo- and pH-sensitive poly(*N*-isopropylacrylamide)/polyaspartic acid IPN hydrogels. Carbohyd Polym 87(4):2425–2431

Liu M, Zeng X, Ma C, Yi H, Ali Z, Mou X, Li S, Deng Y, He N (2017) Injectable hydrogels for cartilage and bone tissue engineering. Bone Res. https://doi.org/10.1038/boneres.2017.14

Miyazaki K, Wintrode PL, Grayling RA, Rubingh DN, Arnold FH (2000) Directed evolution study of temperature adaptation in a psychrophilic enzyme. J Mol Biol 297(4):1015–1026

Qiu L, Liu D, Wang Y, Cheng C, Zhou K, Ding J, Truong VT, Li D (2014) Mechanically robust, electrically conductive and stimuli-responsive binary network hydrogels enabled by superelastic graphene aerogels. Adv Mater. https://doi.org/10.1002/adma.201305359

Qu J, Zhao X, Ma PX, Guo B (2018) Injectable antibacterial conductive hydrogels with dual response to an electric field and pH for localized "smart" drug release. Acta Biomater 72:55–69

Quan C, Zhang Z, Liang P, Zheng J, Wang J, Hou Y, Tang Q (2019) Bioactive gel self-assembled from phosphorylate biomimetic peptide: a potential scaffold for enhanced osteogenesis. Int J Biol Macromol 121:1054–1060

Raia NR, Partlow BP, McGill M, Kimmerling EP, Ghezzi CE, Kaplan DL (2017) Enzymatically crosslinked silk-hyaluronic acid hydrogels. Biomaterials 131:58–67

Shi X, Zheng Y, Wang G, Lin Q, Fan J (2014) pH- and electro-responsive characteristics of bacterial cellulose nanofiber sodium alginate hybrid hydrogels for the dual controlled drug delivery. RSC Adv. https://doi.org/10.1039/C4RA09640A

Singh NK, Lee DS (2014) In situ gelling pH- and temperature-sensitive biodegradable block copolymer hydrogels for drug delivery. J Control Release 193:214–227

Treece MA, Zhang W, Moffitt RD, Oberhauser JP (2007) Twin-screw extrusion of polypropylene-clay nanocomposites: influence of masterbatch processing, screw rotation mode, and sequence. Polym Eng Sci 47(6):898–911

Tuncaboylu DC, Sari M, Oppermann W, Okay O (2011) Tough and self-healing hydrogels formed via hydrophobic interactions. Macromolecules 44(12):4997–5005

Van TD, Tran NQ, Nguyen DH, Nguyen CK, Tran DL, Nguyen PT (2016) Injectable hydrogel composite based gelatin-PEG and biphasic calcium phosphate nanoparticles for bone regeneration. J Electron Mater. https://doi.org/10.1007/s11664-016-4354-3

Wang C, Wang X, Dong K, Luo J, Zhang Q, Cheng Y (2016a) Injectable and responsively degradable hydrogel for personalized photothermal therapy. Biomaterials 104:129–137

Wang R, Zhou B, Xu D, Xu H, Liang L, Feng X, Ouyang P, Chi B (2016b) Antimicrobial and biocompatible epsilon-polylysine-gamma-poly(glutamic acid)-based hydrogel system for wound healing. J Bioact Compat Pol 31(3):242–259

Wang C, Zhang Q, Wang X, Chang H, Zhang S, Tang Y, Xu J, Qi R, Cheng Y (2017) Dynamic modulation of enzyme activity by near-infrared light. Angew Chem Int Edit 56(24):6767–6772

Xing R, Liu K, Jiao T, Zhang N, Ma K, Zhang R, Zou Q, Ma G, Yan X (2016) An injectable self-assembling collagen-gold hybrid hydrogel for combinatorial antitumor photothermal/photodynamic therapy. Adv Mater 28(19):3669–6054

Yang C, Gao L, Liu X (2019) Injectable Schiff base polysaccharide hydrogels for intraocular drug loading and release. J Biomed Mater Res A 107(9):1909–1916

Yesilyurt V, Webber MJ, Appel EA, Godwin C, Langer R, Anderson DG (2016) Injectable self-healing glucose-responsive hydrogels with pH-regulated mechanical properties. Adv Mater. https://doi.org/10.1002/adma.201502902

Zhang X, Liu J, Gao Y, Hao J, Hu J, Ju Y (2019) Multi-stimuli-responsive hydrogels of gluconamide-tailored anthracene. Soft Matter 15(23):4662–4668

Zhao Y, Su H, Fang L, Tan T (2005) Superabsorbent hydrogels from poly(aspartic acid) with salt-, temperature- and pH-responsiveness properties. Polymer 46(14):5368–5376

Zheng W, Chen LJ, Yang G, Sun B, Wang X, Jiang B, Yin GQ, Zhang L, Li X, Liu M, Chen G, Yang HB (2016) Construction of smart supramolecular polymeric hydrogels cross linked by discrete organoplatinum(II) metallacycles via post assembly polymerization. J Am Chem Soc 138(14):4927–4937

Zrinyi M, Gyenes T, Juriga D, Kim JH (2013) Volume change of double cross-linked poly(aspartic acid) hydrogels induced by cleavage of one of the crosslinks. Acta Biomater 9(2):5122–5131

Publisher's Note